Synthetic Mitochondria-Targeting Peptides Incorporating α-Aminoisobutyric Acid with a Stable Amphiphilic Helix Conformation in Plant Cells

AUTHOR(S):

Terada, Kayo; Gimenez-Dejoz, Joan; Kurita, Taichi; Oikawa, Kazusato; Uji, Hirotaka; Tsuchiya, Kousuke; Numata, Keiji

CITATION:

Terada, Kayo ...[et al]. Synthetic Mitochondria-Targeting Peptides Incorporating α-Aminoisobutyric Acid with a Stable Amphiphilic Helix Conformation in Plant Cells. ACS Biomaterials Science & Engineering 2021, 7(4): 1475-1484

ISSUE DATE:

2021-04-12

URL:

http://hdl.handle.net/2433/276532

ACS Biomaterials SCIENCE & ENGINEERING

pubs.acs.org/journal/abseba Article

Synthetic Mitochondria-Targeting Peptides Incorporating α-Aminoisobutyric Acid with a Stable Amphiphilic Helix Conformation in Plant Cells

Kayo Terada, Joan Gimenez-Dejoz, Taichi Kurita, Kazusato Oikawa, Hirotaka Uji, Kousuke Tsuchiya,* and Keiji Numata*

Cite This: *ACS Biomater. Sci. Eng.* 2021, 7, 1475−1484 Read Online

ACCESS | Metrics & More | Article Recommendations | Supporting Information

ABSTRACT: In the genetic modification of plant cells, the mitochondrion is an important target in addition to the nucleus and plastid. However, gene delivery into the mitochondria of plant cells has yet to be established by conventional methods, such as particle bombardment, because of the small size and high mobility of mitochondria. To develop an efficient mitochondria-targeting signal (MTS) that functions in plant cells, we designed the artificial peptide $(LURL)_3$ and its analogues, which periodically feature hydrophobic α-aminoisobutyric acid (Aib, U) and cationic arginine (R), considering the consensus motif recognized by the mitochondrial import receptor Tom20. Circular dichroism measurements and molecular dynamics simulation studies revealed that $(LURL)_3$ had a propensity to form a stable α-helix in 0.1 M phosphate buffer solution containing 1.0 wt % sodium dodecyl sulfate. After internalization into plant cells via particle bombardment, $(LURL)_3$ revealed highly selective accumulation in the mitochondria, whereas its analogue $(LARL)_3$ was predominantly located in the vacuoles in addition to mitochondria. The high selectivity of $(LURL)_3$ can be attributed to the incorporation of Aib, which promotes the hydrophobic interaction between the MTS and Tom20 by increasing the hydrophobicity and helicity of $(LURL)_3$. The present study provided a prospective mitochondrial targeting system using the simple design of artificial peptides.

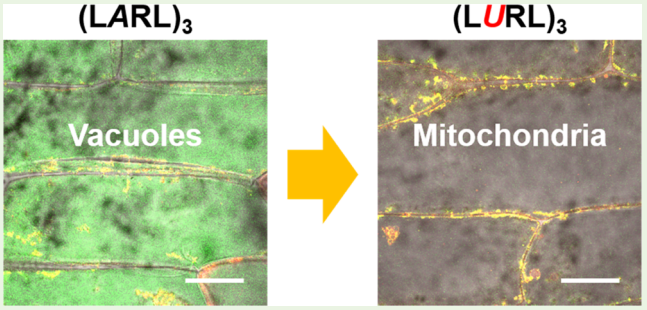

KEYWORDS: *α-aminoisobutyric acid, amphiphilic helix, synthetic mitochondria-targeting peptide, Tom20-recognition consensus sequence*

INTRODUCTION

Mitochondria are the organelles that generate most of the adenosine triphosphate (ATP) in cells and are thus known as the "metabolic powerhouse of the cell".[1] The vital roles of mitochondria involve respiration, cell signaling, differentiation, and regulation of the cell cycle as well as cell growth.[2] Mitochondria are therefore regarded as an attractive target for genetic modification. Plant cells have the potential to produce valuable small molecules such as pharmaceutical medicines, cosmetics, dyes, flavors, and other secondary metabolites that can be synthetically altered to obtain such compounds.[3] Thus, mitochondrial genetic modification is required for increasing secondary metabolite production in terms of ATP production for plant cell factories. In addition, plant mitochondria are a crucial target for increasing agronomic performance, since the associated genes for cytoplasmic male sterility (CMS),[4] which is one of the most widely utilized systems for cross-breeding in the agricultural sector, are encoded by mitochondrial DNA. Although great effort has been devoted to the modification of plant mitochondria to date, the practical modification of the plant mitochondrial genome remains challenging, unlike the genetic modification of other organelles, such as the nucleus and plastids. Conventional methods for the genetic modification of plants, such as agrobacterium-mediated transformation, are mainly applicable for nucleic genomes. Another well-established method for plant genetic modification is particle bombardment,[5−7] which has no dependency on bacteria and no limitations by cell type and species unlike agrobacterium-mediated transformation. In genetic engineering using this technique, DNAs are coated onto the surface of micro-sized metal particles such as tungsten and gold via deposition by spermidine and calcium chloride and directly accelerated into cells as being carried on the particles by high-pressure gas. Subsequently, the DNA elute off inside the cells and a portion of them might participate in the transformation.

Received: October 28, 2020
Accepted: February 11, 2021
Published: February 19, 2021

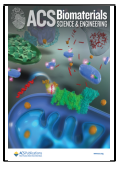

https://dx.doi.org/10.1021/acsbiomaterials.0c01533
ACS Biomater. Sci. Eng. 2021, 7, 1475−1484

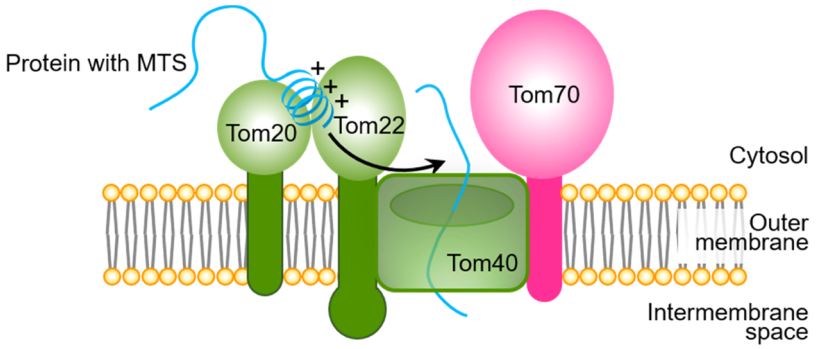

Figure 1. Mitochondrial preprotein import pathway. Most mitochondrial proteins are encoded in the nuclear genome and synthesized in the cytosol with a mitochondrial targeting sequence at the N-terminus of the proteins. The preproteins are translocated through the TOM complex. Mitochondrial targeting sequences adopting an amphiphilic helical conformation are recognized by Tom20 and Tom22 via hydrophobic and electrostatic interactions, respectively.

Gold particles are generally used as macrocarriers to date because of their uniform particle size, spherical shape, high purity, as well as lower toxicity compared with other metal particles such as tungsten.[8,9] In addition, gold does not affect the formulation of the substrate coated on the particles for a long term. Owing to the direct internalization mechanism into the cytosol, particle bombardment has been applied to gene delivery into other organelles than nuclei, such as plastids,[10,11] and selective translocation in mitochondria has not been achieved because of their characteristics, such as a small size of approximately 1 μm and extremely fast movement in the cytosol. We have recently reported mitochondria-targeting gene delivery in plants such as *Arabidopsis thaliana*[12] and *Nicotiana tabacum*[13] as well as in human embryonic kidney (HEK) 293 cells[14] using the mitochondrial targeting signal (MTS)-fused peptide, where the first 12 residues of the presequence (Cytcox) in the yeast cytochrome *c* oxidase subunit IV are fused to lysine−histidine (KH) peptide. The helical conformation of this fused peptide was found to be necessary for effective mitochondrial import, similar to most MTSs. However, the efficiency of gene delivery efficiency into mitochondria using this system is still too low for the stable transfection of plant cells.

Mitochondria contain more than 1000 types of proteins, most of which are encoded in the nuclear genome. Mature proteins with endogenous signals, including MTSs, are synthesized in the cytosol and subsequently translocated into the appropriate organellar compartments, such as the mitochondrial outer membrane, intermembrane space, inner membrane, and matrix.[15] The import pathway via MTSs is mediated by several membrane-associated receptors, namely, the translocase of the outer mitochondrial membrane (TOM), the translocase of the inner mitochondrial membrane (TIM), and the sorting and assembly machinery (SAM). Among the proteins in the TOM complex, Tom40 is the channel-forming β-barrel protein, and the associated proteins Tom20, Tom22, and Tom70 are single-pass transmembrane proteins anchored to each other at their N-terminus by the cytosolic domains (Figure 1).[16−19] At the first step of import, MTSs are recognized by the cytosolic domains of Tom20 and Tom22 via hydrophobic and electrostatic interactions, respectively (Figure 1).[20] MTSs are ∼15 to 70 residues in length and form amphiphilic helical structures that have positively charged basic residues. Lee et al. have proven that the N-terminal domain of mitochondrial preprotein carrying hydrophobic and multiple-arginine sequences was the mitochondrial specificity factor via mutation of the N-terminal domain of the Rubisco small subunit.[21] Furthermore, the Tom20-recognition segments of MTSs, including Cytcox, have also been determined to correspond to the helical region.[22] The fact that the amphiphilic helix with hydrophobic and cationic faces is critical for recognition by Tom20 and Tom22 motivated us to stabilize the helical conformation of peptides to enhance specific mitochondrial accumulation.

The incorporation of α,α-disubstituted α-amino acids (dAAs), such as α-aminoisobutyric acid (Aib), is a useful method for inducing and stabilizing helical conformations of peptides.[23−28] It has been reported that amphiphilic cell-penetrating peptides (CPPs) containing dAAs form stable helices, which enhance peptide uptake efficiency.[29−33] We have also reported that Aib-containing CPPs adopting helical conformations exhibit long-term internalization into both mammalian and plant cells with higher efficiency than conventional CPPs.[34]

Here, we designed novel artificial amphiphilic peptides containing Aib residues to develop highly efficient MTSs applicable for plant cells by taking a Tom20-recognition consensus sequence into account. The consensus sequence of MTSs has been recently explored in terms of the Tom20-recognition site. Obita et al. deduced that the reasonable consensus motif $\sigma\varphi\chi\beta\varphi\varphi$ (σ: hydrophilic; φ: hydrophobic; β: basic; χ: any amino acid) imparts strict recognition by Tom20 to MTSs by estimating the relative affinity between the cytosolic domain of Tom20 and the various peptides derived from the presequence of aldehyde dehydrogenase (ALDH).[35] We thus prepared four types of peptides, $(LARL)_3$, $(LURL)_3$, $(LURR)_3$, and $(LURS)_3$, with sequences that periodically include cationic and hydrophobic amino acids, to develop novel mitochondrial targeting peptides with high accumulation ability in plant cell mitochondria (Figure 2a,b). The Tom20-recognition consensus motif containing the Aib residue is involved in periodic sequences, which are expected to strongly interact with Tom20 in the form of a stable amphiphilic helix. All four peptides were fluorescently labeled with fluorescein (FAM) to investigate the intracellular localization using confocal laser scanning microscopy (CLSM) in plant cells (Figure 2c).

MATERIALS AND METHODS

Materials. Peptides labeled with FAM at the N-terminus were synthesized by the Research Resources Center of RIKEN Brain Science Institute. The chemical structure of FAM is shown in Figure

https://dx.doi.org/10.1021/acsbiomaterials.0c01533
ACS Biomater. Sci. Eng. 2021, 7, 1475−1484

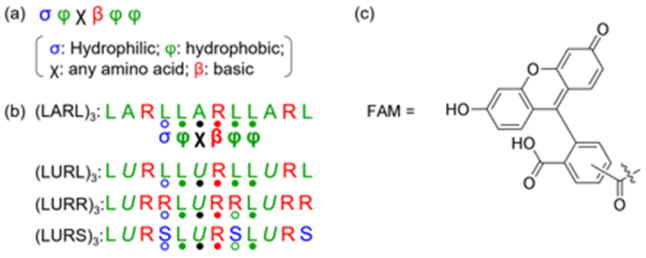

Figure 2. (a) Tom20-recognition consensus motif reported in the literature.[35] (b) Peptide sequences containing the Tom20-recognition consensus motif. U indicates α-aminoisobutyric acid (Aib). (c) Structure of the fluorescent probe FAM (5- and 6-carbosyfluorescein).

2c. Reversed-phase high-performance liquid chromatography (RP-HPLC) analyses were performed to characterize FAM-labeled peptides with the mobile phase composed of Milli-Q water containing 0.1% (v/v) trifluoroacetic acid (TFA) (eluent A) and acetonitrile containing 0.1% (v/v) TFA (eluent B) (Figure S1). For $(LARL)_3$ and $(LURL)_3$, the composition of the mobile phase changed from 60% A and 40% B to 30% A and 70% B over 30 min in a linear gradient mode at a flow rate of 1 mL min^{-1}. For $(LURR)_3$, the composition altered gradually from 80% A and 20% B to 50% A and 50% B over 30 min at 1 mL min^{-1}. For $(LURS)_3$, the composition altered gradually from 70% A and 30% B to 40% A and 60% B over 30 min at 1 mL min^{-1}. The column temperature was kept at 25 °C, and elution of the various compounds was monitored by ultraviolet (UV) absorbance at 220 nm. The matrix-assisted laser desorption ionization time-of-flight (MALDI-TOF) mass spectra of FAM-labeled $(LARL)_3$, $(LURL)_3$, $(LURR)_3$, and $(LURS)_3$ are shown in Figure S2. MitoTracker Red CMXRos (MTR) was purchased from Invitrogen by Thermo Fisher Scientific (Waltham, MA). Onion bulbs (*Allium cepa*) were purchased from the supermarket (Saitama, Japan). The onion was stored at 4 °C and rewarmed to room temperature before being subjected to particle bombardment. Gold particles (0.6 μm diameter) were purchased from Bio-Rad Laboratories (München, Germany).

Circular Dichroism (CD) Spectroscopy. The CD spectra of FAM-labeled peptides (25 μM) in phosphate-buffered saline (PBS, 0.1 M) containing 1.0 wt % sodium dodecyl sulfate (SDS) were acquired at 25 °C using a Jasco J-820 CD spectropolarimeter (Jasco, Tokyo, Japan). Background scans were obtained for PBS containing 1.0 wt % SDS. Measurements were performed using a quartz cuvette with a 0.1 cm path length. Each spectrum represents the average of 10 scans from 190 to 250 nm with a 0.2 nm resolution, obtained at 50 nm min^{-1} with a bandwidth of 1 nm. The secondary structure contents of each peptide were calculated by the DichroWeb online CD analysis server using CDSSTR algorithms in combination with reference dataset 6, optimized for data in the range of 190−240 nm.

Dynamic Light Scattering (DLS). DLS measurements of FAM-labeled peptides (25 μM) in 0.1 M PBS containing 1.0 wt % SDS were performed at 25 °C using a zeta potentiometer (Zetasizer Nano-ZS, Malvern Instruments, U.K.) and a DTS1070 folded capillary cell (Malvern Panalytical).

Molecular Dynamics (MD) Simulations. *Folding of the Peptides by Classical Molecular Dynamics.* The tLeap module from the AMBER 16 package[36] was used to construct the starting structures of the $(LARL)_3$, $(LURL)_3$, $(LURR)_3$, and $(LURS)_3$ peptides. The parameters used for describing the Aib residue were taken from the literature,[37] and the other residues were described using the AMBER ff14SB force field.[38] The systems were solvated in a TIP3P[39] water box, and counterions were added. The SHAKE algorithm[40] was used to restrain the bonds with hydrogen atoms and allow a time step of 2 ps for the simulations, and periodic boundary conditions were used. The constant temperature was set to 300 K, and the pressure was set to 1 atm using a weak-coupling algorithm.[41] Electrostatic interactions were calculated using particle mesh Ewald (PME) summation[42] with a cutoff of 8.0 Å for long-range interactions. The systems were water energy-minimized for 5000 steps using the conjugate gradient minimization algorithm with the solute atoms constrained with an energy of 50 kcal mol^{-1}; then, the constraints were removed from the solute, and all of the system was energy-minimized for 10 000 steps with the conjugate gradient minimization algorithm. Afterward, the systems were slowly heated to 300 K over 600 ps with the solute atoms fixed with a 2 kcal mol^{-1} restraint. Then, the system was equilibrated in the NVT ensemble over 500 ps to ensure the appropriate density of the water box.

Next, each peptide was subjected to classical molecular dynamics (cMD), and all simulations were carried out using AMBER. For each peptide, eight replicas were initiated from the initial equilibrated structure and run using GPUs[43−45] in the Hokusai Supercomputer. The simulation time for each replica was approximately 300 ns, giving an accumulated simulation time for each peptide of approximately 2.4 μs. Analysis of the simulations was carried out using CPPTRAJ,[46] and cluster analysis was performed with the DBSCAN algorithm.[47]

Peptides and Tom20: Construction. The Tom20 structure was taken from the structure of rat Tom20 bound to the rat ALDH presequence LSRLL motif (PDB ID: 2v1t).[48,49] The selenium methionine present in Tom20 was mutated to a methionine. The rat ALDH presequence motif was used to align the folded peptide structures ($(LARL)_3$, $(LURL)_3$, $(LURR)_3$, and $(LURS)_3$) obtained from the previous simulations, and then the rat ALDH presequence motif was removed. The systems were constructed using the tLeap module of AMBER 16[36] using the same Aib parameters taken from,[37] and the AMBER ff14SB force field was used for all other residues.[38] The systems were solvated in a water box of TIP3P[39] molecules and counterions. The SHAKE algorithm[40] was used, and a time step of 2 ps was used for the simulations. Boundary conditions were applied, and constant temperature and pressure were set to 300 K and 1 atm using a weak-coupling algorithm.[41] Electrostatic interactions were calculated using particle mesh Ewald (PME) summation[42] with a cutoff of 8.0 Å for long-range interactions.

Peptides and Tom20: Equilibration. The systems were water energy-minimized for 5000 steps using the conjugate gradient minimization algorithm with the solute atoms constrained with an energy of 50 kcal mol^{-1}; then, the constraints were removed from the solute, and the whole system was energy-minimized for 10 000 steps with the conjugate gradient minimization algorithm. Afterward, the systems were equilibrated in a series of steps in which the force applied to the atoms of the solute slowly decreased. First, the systems were slowly heated from 0 to 300 K over 600 ps with the solute atoms fixed with a force of 2 kcal mol^{-1}. Then, the system was equilibrated in the NVT ensemble over 500 ps with the solute atoms fixed with a constraint of 0.5 kcal mol^{-1}. A distance restraint of 18 Å from the center of mass (COM) of the peptide to the COM of Tom20 was applied during the equilibration of the system.

Peptides and Tom20: Gaussian Accelerated Molecular Dynamics (GaMD). Gaussian accelerated molecular dynamics (GaMD)[50] simulations were performed to increase sampling of the system. For each peptide, three different starting positions with regard to Tom20 were used, and for each of these starting structures, three replicas were run (each peptide had a total of nine simulations). An initial MD simulation of 24 ns was performed for each system to obtain the initial parameters and system potential needed for the GaMD. After that, GaMD simulations were run using dual-boost acceleration. Production GaMD simulations were conducted with the system threshold energy set to $E = V_{max}$. All peptide replicas were run for approximately 200 ns, giving an accumulated GaMD time of approximately 1.8 μs for each peptide. CPPTRAJ was used to analyze the simulations. The distance between the Cα carbons of the initial and final amino acids of the peptides together with the distance from the COM of the peptide to the COM of the side chains of the Tom20 site 1[48] residues (Ile21, Leu53, and Leu57) were used for the reweighting and analysis of the free-energy landscape (FEL). The reweighted simulations were performed using the PyReweighting toolkit[51] to calculate the two-dimensional (2D) potential of mean force (PMF) profiles, and a bin of 0.2 and a cutoff of 50 were used. Cluster analysis was performed with the DBSCAN algorithm.

https://dx.doi.org/10.1021/acsbiomaterials.0c01533
ACS Biomater. Sci. Eng. 2021, 7, 1475−1484

Proteolytic Stability Assay. A 10 mM phosphate buffer solution (pH 7.2) containing a polypeptide (0.1 mg mL^{-1}) and trypsin (1 μg mL^{-1}) was incubated at 37 °C with shaking at 900 rpm. After several hours, 60 μL of the peptide solution was poured into 150 μL of 1% TFA to deactivate the trypsin. After the addition of 30 μL of Boc-Gly solution (2.5 mg mL^{-1}) as an internal standard, the mixture was centrifuged at 13 500 rpm to precipitate the deactivated trypsin. The supernatant was analyzed by RP-HPLC to determine the amount of residual polypeptides based on the peak areas. RP-HPLC analyses were performed with the mobile phase composed of Milli-Q water containing 0.1% (v/v) TFA (eluent A) and acetonitrile containing 0.1% (v/v) TFA (eluent B). The composition of the mobile phase changed from 95% A and 5% B to 0% A and 100% B over 47.5 min in a linear gradient mode at a flow rate of 1 mL min^{-1}.

Preparation of Clean Gold Particles. A gold nanocarrier (30 mg, 0.6 μm) was weighed into a 1.5 mL Eppendorf tube, and then 1 mL of ice-cold 70% ethanol was added. The tube was shaken vigorously in a vortex mixer for 5 min and then settled for 15 min at 25 °C. The tube was subjected to centrifugation at 2000*g* for 5 s to sediment and compact the gold. The supernatant was removed, and then 1 mL of ice-cold sterile distilled water was added. The gold particles were resuspended by vortexing and allowed to settle at 25 °C for 10 min. The gold particles were then compacted by centrifugation at 2000*g* for 5 s. The supernatant was removed, and 1 mL of ice-cold sterile distilled water was added. The gold particles were resuspended by vortexing and then allowed to settle at 25 °C for 10 min. The gold particles were washed again with water according to the same protocol as above. The tube was subjected to centrifugation at 2000*g* for 15 s, and the water was then removed completely. Next, 500 μL of 50% glycerol was added, and the tube was vortexed for 1 min to resuspend the gold particles. While the tube was shaken, the suspension of the gold particles was divided into ten 1.5 mL aliquots in Eppendorf tubes to prepare the stable stock suspension of gold particles. The clean gold particles were stored at −80 °C.

Peptide Coating on Gold Particles for Particle Bombardment. Before using the stored gold particles, the tube was vortexed for 5 min. While the tube containing the clean gold particles prepared as described above was shaken, 2 μL of FAM-labeled peptide solution in dimethyl sulfoxide (DMSO) (20 mM) and 150 μL of water were subsequently added. The tube was shaken by vortexing for 5 min. The gold particles coated with FAM-labeled peptide were sedimented by centrifugation at 2000*g* for 5 s. The supernatant was removed, and 50 μL of water was added. The gold particles were suspended by gentle pipetting and then sedimented by centrifugation at 2000*g* for 5 s. The supernatant was removed, and the gold particles were resuspended in 50 μL of 70% ethanol.

Improved Coating Method on Gold Particles for $(LURR)_3$ and $(LURS)_3$. The clean gold particles were subsequently washed with 150 μL of 70% ethanol and 150 μL of 100% ethanol to remove glycerol. Ethanol (150 μL, 100%) was added to the tube, and the gold particles were resuspended by vortexing. While the tube was shaken by vortexing, 2 μL of FAM-labeled peptide solution in DMSO (20 mM) was used to deposit peptide on the surface of the gold particles. The tube was shaken for 5 min and then subjected to centrifugation at 2000*g* for 5 s. The supernatant was removed, and the gold particles were resuspended in 50 μL of acetonitrile.

Particle Bombardment for Onion Bulbs. The gold suspension (10 μL) coated with FAM-labeled peptides was loaded onto a macrocarrier, which was then dried in air. The second or third onion bulb scale leaves were cut into pieces of approximately 2 cm × 3 cm and placed on a wet filter paper in a 9 cm Petri dish. Bombardment was performed with a 650 psi rupture disk and 28 in. Hg of vacuum pressure. After bombardment, a layer of the epidermal cells of the onion scale leaves was stripped and soaked in an aqueous solution of MTR (1 μM) for 30 min at 25 °C.

Immunostaining of Cut Tissues of Onion Bulb Scale. "Solution A" was prepared with the composition of 5 mM 2-(*N*-morpholino)ethanesulfonic acid (MES) buffer, 0.4 M mannitol, and 70 mM $CaCl_2$ prior to the experiment. Onion bulb scales were cut into slices and then incubated with a solution of FAM-$(LURL)_3$ in solution A (0.1 mg mL^{-1}, 1% DMSO) for 6 h. The peptide-treated tissues were fixed with 4% paraformaldehyde in solution A for 30 min and then permeabilized in solution A containing 0.9% NaCl, 0.25% gelatin, 0.02% SDS, and 0.1% Triton X-100 for 10 min. Fixed tissues were washed with solution A and then incubated with anti-Tom20 antibody in solution A followed by tetramethylrhodamine isothiocyanate (TRITC)-labeled anti-rabbit IgG in solution A as a secondary antibody.

Confocal Laser Scanning Microscopy (CLSM) Observation. The intracellular colocalization studies were performed by CLSM (LSM 880, Carl Zeiss, Oberkochen, Germany). Images were acquired at excitation wavelengths of 488 nm (for FAM) and 555 nm (for MTR) and visualized under a 20× or 63× oil immersion objective. Colocalization analysis of micrographs was performed using Zen 2011 operating software.

RESULTS AND DISCUSSION

Secondary Structures of the Peptides. The CD spectra of four types of FAM-labeled peptides were measured in PBS (0.1 M, pH 7) containing 1.0% SDS to define the secondary structures in the vicinity of the lipophilic biomembranes, including mitochondrial membranes (Figure 3). FAM-

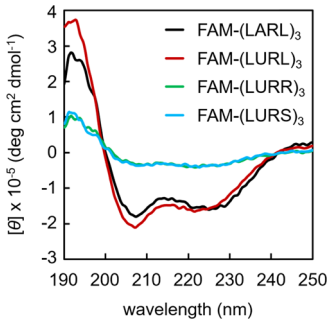

Figure 3. CD spectra of the FAM-labeled peptides measured 0.1 M PBS (pH 7) containing 1.0% SDS (c = 25 μM) at 25 °C.

$(LARL)_3$, FAM-$(LURL)_3$, FAM-$(LURR)_3$, and FAM-$(LURS)_3$ exhibited negative peaks at 222 and 207 nm and a positive peak at 192 nm, which is typical of a helical conformation, although their intensities were quite varied. The CD signals of FAM-$(LARL)_3$ and FAM-$(LURL)_3$ were much stronger than those of FAM-$(LURR)_3$ and FAM-$(LURS)_3$, suggesting that FAM-$(LARL)_3$ and FAM-$(LURL)_3$ have a higher propensity to form helical structures than FAM-$(LURR)_3$ and FAM-$(LURS)_3$. The predominant helical structure of peptides is experimentally estimated by the intensity ratio of the signals at 222 and 207 nm ($[\theta]_{222}/[\theta]_{207}$, R ratio).[52−54] Judging from the R ratios of FAM-$(LARL)_3$, FAM-$(LURL)_3$, FAM-$(LURR)_3$, and FAM-$(LURS)_3$ (0.78, 0.86, 1.27, and 1.07, respectively), their predominant conformation is considered to be an α-helix. It has been previously reported that Aib-containing peptides with long sequences (the number of total amino acid residues ≥9) preferentially adopt an α-helix rather than a 3_{10} helix.[55] Since the four peptides in this study contain 12 residues, their conformation is expected to be an α-helix, which is consistent with the conformation estimated on the basis of the R ratios. The CD spectroscopic data at pH 7 were analyzed with DichroWeb, an online server for protein secondary structure analyses, using CONTIN[56] as an algorithm to estimate the contents of the secondary structures. The results are summarized in Table S1. Helical conformations were obviously

https://dx.doi.org/10.1021/acsbiomaterials.0c01533
ACS Biomater. Sci. Eng. 2021, 7, 1475−1484

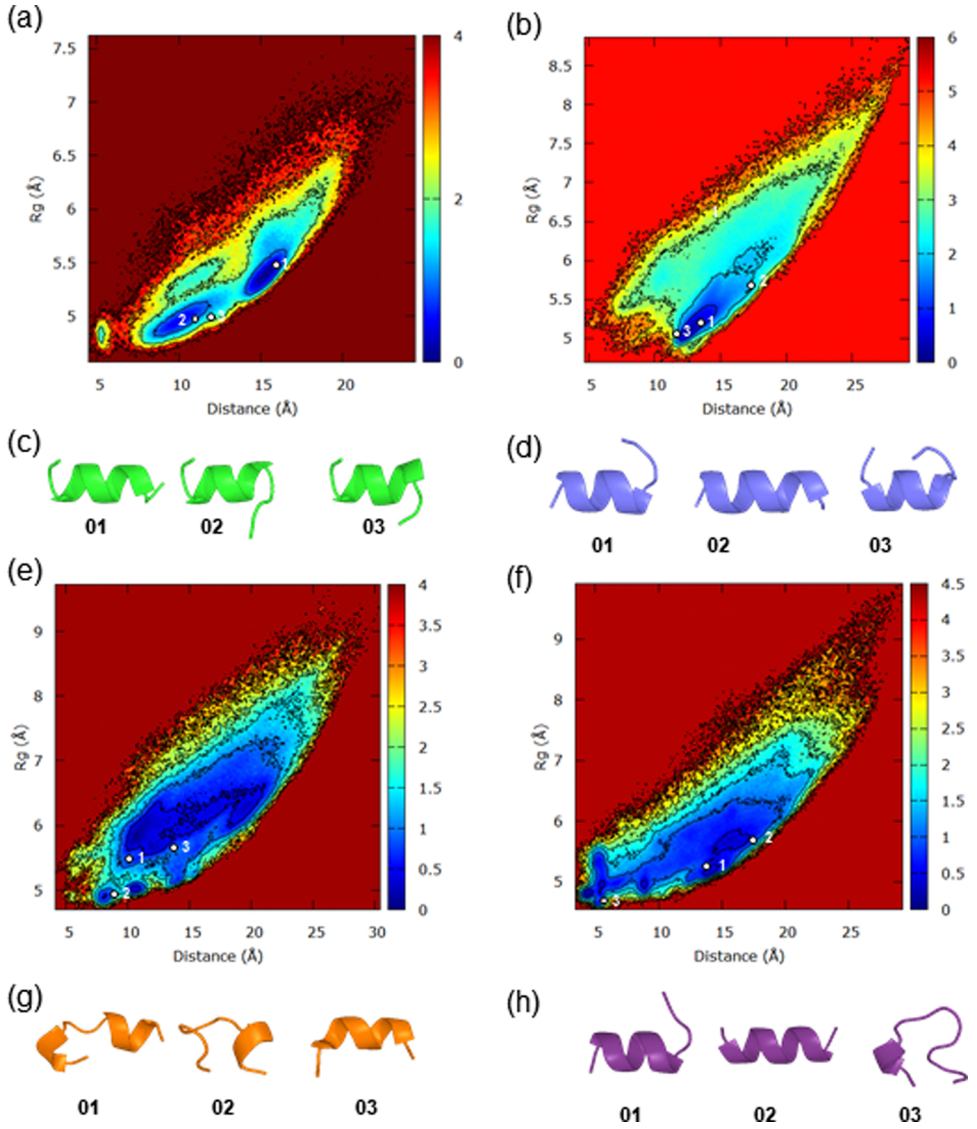

Figure 4. (a, b) Free-energy landscape of the end-to-end distance vs the radius of gyration (R_g) of the model sequence calculated from classical MD simulations for $(LARL)_3$ (a) and $(LURL)_3$ (b). (c, d) Representative structures of each cluster for $(LARL)_3$ (c) and $(LURL)_3$ (d). (e, f) Free-energy landscape of the end-to-end distance vs R_g of the model sequence calculated from classical MD simulations for $(LURR)_3$ (e) and $(LURS)_3$ (f). (g, h) Representative structures of each cluster for $(LURR)_3$ (g) and $(LURS)_3$ (h). The deepest blue regions in the free-energy landscapes of (a), (b), (e), and (f) indicate the energy minima. Colors represent energy in kcal mol^{-1}. The cluster numbers for (c), (d), (g), and (h) are given in the free-energy landscapes of (a), (b), (e), and (f), respectively.

predominant for all of the peptides. In addition, the pH responsiveness of the peptide conformation was evaluated.

The CD spectra of FAM-$(LARL)_3$ and FAM-$(LURS)_3$ barely changed in the pH range from 4 to 9 (Figure S3). On the other hand, the ratio of the signal intensity at 207 nm to that at 222 nm gradually increased with an isosbestic point at approximately 215 nm as the pH decreased in the cases of FAM-$(LURL)_3$ and FAM-$(LURR)_3$. In the DLS measurements in PBS (0.1 M, pH 4 and 7) containing 1.0% SDS, large aggregation of the helices was not found for all of the peptides despite their amphiphilic nature (Figure S4). The double-minimum pattern with a stronger negative intensity at the longer wavelength in a CD spectrum is typical for helix bundles.[57−59] The spectroscopic changes in CD spectra of FAM-$(LURL)_3$ and FAM-$(LURR)_3$ suggest that the formation of α-helical bundles was facilitated, which was probably triggered by the partial protonation of the carboxylates at the C-termini of peptides at lower pH. This bundle formation would be due to the intermolecular hydrophobic interaction of the hydrophobic faces of $(LURL)_3$ or $(LURR)_3$, implying the strong amphiphilicity of their helices owing to the substitution of Aib residues for alanine residues. The DLS results indicate that the helix bundles formed from $(LURL)_3$ or $(LURR)_3$ comprise a small number of peptide chains.

To corroborate the results obtained by CD measurements, we constructed the model structures of all of the peptides and conducted molecular dynamics simulations to predict their folding structures. Since the fluorescent labels do not affect the secondary structures of their binding peptides, the structure of FAM was omitted from the model structures to simplify the calculation. The free-energy landscapes of the peptides using the end-to-end distance vs the radius of gyration (R_g) as variables for the model sequences of $(LARL)_3$, $(LURL)_3$, $(LURR)_3$, and $(LURS)_3$ are shown in Figure 4. The most

https://dx.doi.org/10.1021/acsbiomaterials.0c01533
ACS Biomater. Sci. Eng. 2021, 7, 1475−1484

populated structures of $(LARL)_3$ and $(LURL)_3$ took helical conformations in the major clusters, corresponding to clear energy minima in the free-energy landscape. In contrast, $(LURS)_3$ and $(LURR)_3$ adopted less α-helical conformations during the entire simulation time, as shown by the broader energy minima in the FEL without a stable minimum and by the peptide structures found in the major clusters, which present fewer α-helical conformations (Figure S5). These simulation results agree well with the CD analyses.

Proteolytic Stability of the Peptides. The incorporation of nonproteinogenic amino acid including Aib into peptides is known to improve the tolerance to the enzymatic degradation of the peptides. We previously demonstrated that the Aib-containing CPPs had higher resistance against the enzymatic degradation over a long period compared to the representative CPPs, human immunodeficiency virus (HIV)-1-derived Tat peptide, in mammalian and plant cells.[34] When CPPs are subjected to plant cells, long-term stability to enzymatic degradation is crucial because CPPs are considered to stay in the intercellular spaces after internalization into plant tissues.[60,61] Mitochondrial targeting peptides could also suffer the degradation in endosomes or vacuoles as well as in the intracellular spaces in practical use. Therefore, we examined the stability of the FAM-labeled $(LARL)_3$, $(LURL)_3$, $(LURR)_3$, and $(LURS)_3$ against enzymatic degradation using trypsin, which prefers to digest arginine-containing sequences, as a model enzyme (Figure S6, HPLC data shown in Figures S7−S10). Before trypsin treatment, two distinct peaks were observed corresponded to isomers of the peptides, which are conjugated to FAM at 5- or 6-position. After 1 h incubation with trypsin, 94% of $(LARL)_3$ had degraded, whereas more than 8 h was needed for the complete digestion of $(LURL)_3$. Moreover, $(LURR)_3$ remained almost intact even after 8 h. It suggests that the Aib-incorporation into the peptides improved their tolerance to enzymatic degradation, although $(LURS)_3$ was degraded much faster than the other Aib-containing peptides.

Localization of Peptides in Plant Cells. The mitochondrial targeting ability of the peptides in plant cells was investigated using onion bulb scales. The epidermal cells of the onion have no chlorophyll, leading to easy assessment of peptide localization. Although we first performed the internalization assay for epidermal cells of onion bulb scale leaves using FAM-$(LURL)_3$ by treatment with a solution of the peptide for 16 h, the fluorescence originating from FAM was almost not observed (Figure S11). In general, peptides or proteins without any modification are considered to be hardly internalized into cells due to the obstacles such as cell walls and cell membranes. For their delivery to plant cells, typically, they are conjugated to CPP[62] or encapsulated within CPP-modified micelles or vesicles.[63] Using these internalization methods, the release of peptides or proteins from endosomes into cytosol is required for the mitochondrial targeting after the endocytic uptake, because the peptides or the proteins not going through the endosomal escape would be transferred to the vacuoles and then degraded. Alternatively, particle bombardment using gold particles, which is a well-established method for genetic transformation of plants, is not toxic[9] and can internalize the peptides into the cytosol directly. In addition, the protein delivery with particle bombardment, called "proteolistics" was recently achieved by Martin-Ortigosa and Wang,[64] in which they used gold particles coated with protein instead of DNA. We applied this method by changing proteins into peptides for internalization of the peptides into the cytosol to exclude the difference in the efficiencies of endosomal escape as well as to avoid the influence of the difference in cellular uptake efficiencies of the peptides caused by the cell wall and the cell membrane. We use 0.6 μm of gold particles, which is reported to be appropriate to plant cell transformation. The peptides were coated on the surfaces of gold particles for particle bombardment using the dispersion of the FAM-labeled peptides in pure water. The peptide was precipitated onto the surface of the gold particles through the mixing peptide solution in a good solvent, DMSO, with a poor solvent, water. The various interactions such as hydrophobic interaction, coordination with O or N atoms might be involved in the peptide coating on the surface of the gold particles. Once the peptide-coated gold particles are bombarded into cells, the peptides are eluted off the particles in cytosol and then transferred to each organelle in accordance with the inherent nature of the peptides. In the present study, we evaluated the specificity of the peptides for mitochondria in terms of the intracellular trafficking from cytosol to mitochondria. Although the coating efficiency would be varied depending on the peptide in the coating method noted above, it would hardly affect the selectivity for mitochondria unlike internalization efficiency. CLSM observation was carried out to obtain information about the intracellular localization of the peptides after internalization into the cytosol. The mitochondria of the cells were stained with MTR after the internalization of the peptides into the cytosol via particle bombardment. In the CLSM images of the epidermal cells of onion bulb scale leaves after bombardment of gold particles coated with the FAM-labeled peptides, the fluorescence originating from FAM was dispersed throughout the cells with a relatively stronger intensity in mitochondria for $(LARL)_3$ (Figure 5). This result indicates that $(LARL)_3$ was transferred into vacuoles and mitochondria without any specific localization. On the other hand, the strong fluorescence from FAM was observed and clearly colocalized with that of MTR for $(LURL)_3$, suggesting that $(LURL)_3$ was localized in mitochondria. In contrast, no obvious fluorescent signal was observed for $(LURR)_3$ and $(LURS)_3$, probably due to their low coverage on the surface of gold particles caused by their slightly higher solubility in water under the same coating conditions as $(LARL)_3$ and $(LURL)_3$ (Figure S12). The appropriate coating conditions, especially for $(LURR)_3$, where ethanol was used because pure water was a poor solvent, improved the amounts of $(LURR)_3$ and $(LURS)_3$ internalized into the cells; however, the peptides were localized in vacuoles as well as mitochondria (Figure S13). $(LURL)_3$ has a propensity to form a more stable amphiphilic helix in the membrane-mimicking environment, as deduced from the results of CD measurements, indicating a more efficient interaction with Tom20 and Tom22 than the other peptides. The amphiphilic helical conformation of $(LURL)_3$ stabilized by the incorporation of Aib residues would allow more specific binding to Tom20 and Tom22, which have been reported to recognize hydrophobic and cationic regions of MTSs, respectively.

Molecular Interactions of Peptides with Tom20. Binding simulations of the peptides with Tom20 were conducted using GaMD simulation. We utilized the optimum folded structures obtained from the molecular dynamics simulations of the peptides as the starting point (Figure 6). In the cluster analysis performed with the DBSCAN algorithm,

https://dx.doi.org/10.1021/acsbiomaterials.0c01533
ACS Biomater. Sci. Eng. 2021, 7, 1475−1484

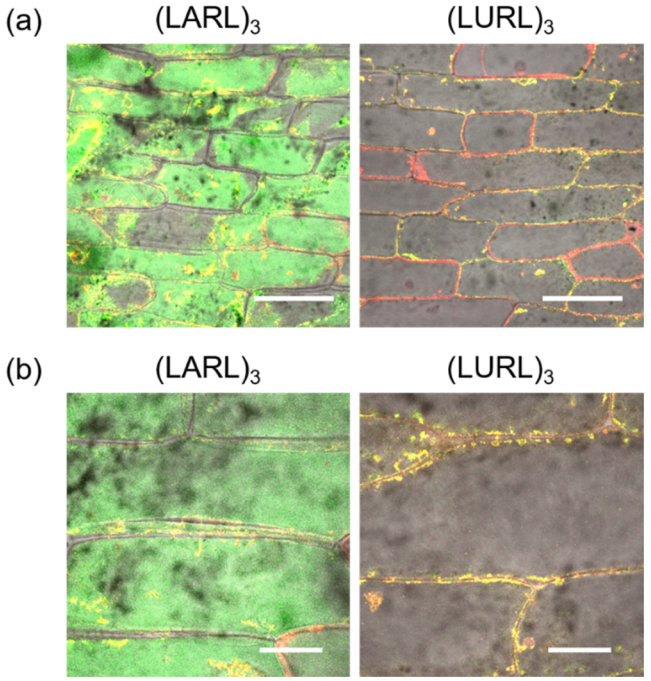

Figure 5. (a) CLSM observation of epidermal cells of onion bulb scales bombarded by gold particles coated with FAM-$(LARL)_3$ and FAM-$(LURL)_3$ (target distance: 6 cm; vacuum: 28 in. Hg; particle size: 0.6 μm; helium pressure: 650 psi). (b) Expanded CLSM images of cells bombarded by gold particles coated with FAM-$(LARL)_3$ and FAM-$(LURL)_3$ under the same conditions as (a). Mitochondria were stained with MTR. Scale bars indicate 200 and 50 μm for (a) and (b), respectively.

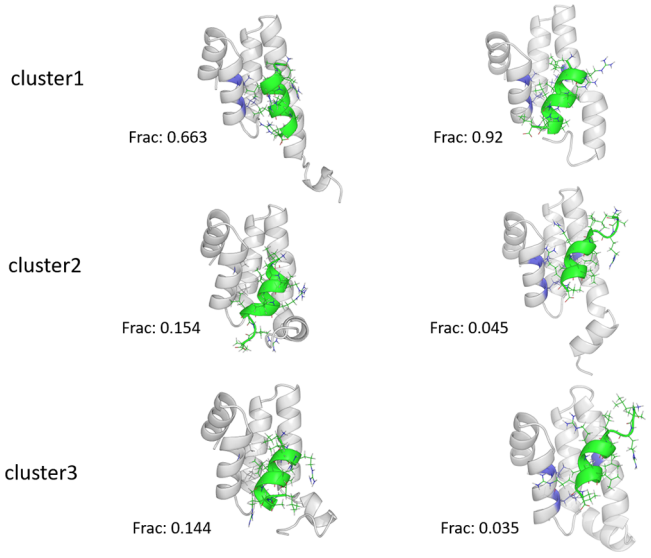

Figure 6. Modeling the interaction between $(LARL)_3$ or $(LURL)_3$ and Tom20 (PDB ID: 2v1t) with the main clusters of the peptides and the size of the cluster as a fraction of the total trajectory found using the DBSCAN algorithm.

the first cluster of $(LURL)_3$ constituted a fraction of 0.92, where $(LURL)_3$ was in an α-helical conformation. In contrast, the first cluster of $(LARL)_3$ occupied a fraction of 0.663, implying that $(LURL)_3$ is in a more stable conformation while binding Tom20 than $(LARL)_3$. In addition, the free-energy landscape shows that the $(LURL)_3$ energy minimum is closer to that of Tom20 (main energy minima at ~7 and 8.5 Å) than the energy minimum of $(LARL)_3$ is (main energy minimum at 9 Å and a small one at 7.5 Å) (Figure S14). Therefore, $(LURL)_3$ would interact with Tom20 more strongly, resulting in the selective mitochondrial accumulation of $(LURL)_3$. We also investigated the molecular recognition of $(LURL)_3$ with Tom20 by immunostaining against Tom20 for $(LURL)_3$ using cut tissues of onion bulb scale to demonstrate selective accumulation into mitochondria of $(LURL)_3$ was ascribed to the molecular recognition by Tom20 (Figure 7). In the CLSM

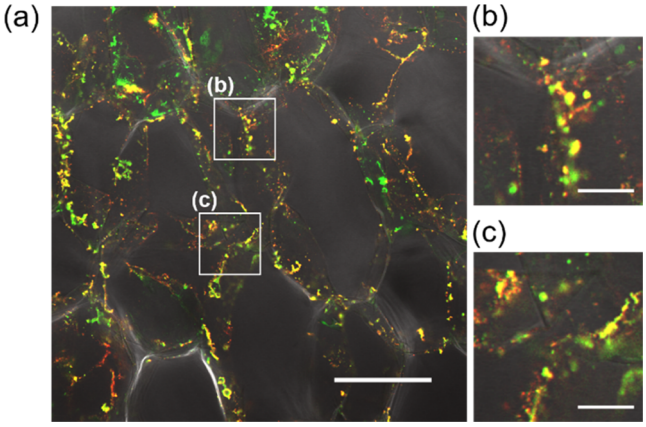

Figure 7. (a) CLSM observation of cut tissue of onion bulb scale leaves treated with FAM-$(LURL)_3$ followed by immunostaining with anti-Tom20 antibody. (b, c) Enlarged images of the boxes in (a). The scale bars represent 100 μm for (a) and 20 μm for (b) and (c). FAM was represented in green color, and TRITC was represented in red color.

image of peptide-internalized cut tissues, many colocalized fluorescent signals of FAM with TRITC were observed, implying the recognition of $(LURL)_3$ by Tom20. We could not evaluate the binding efficiency of $(LURL)_3$ to Tom20 due to the resolution of the CLSM image. However, the preference for $(LURL)_3$ on the molecular recognition by Tom20 was supported by CLSM and in silico results.

The finding that $(LARL)_3$ and $(LURL)_3$ have a stronger tendency to adopt an α-helical conformation than $(LURR)_3$ and $(LURS)_3$ implies that the content of cationic or hydrophilic amino acid residues affects the helical stability more strongly than the incorporation of Aib residues in the current periodic peptides. Considering the low selectivity of $(LURR)_3$ for mitochondria compared to that of $(LURL)_3$ despite the further introduction of the cationic amino acid residue, which is expected to interact with Tom22, the stable amphiphilic helical conformation is assumed to be essential for effective interaction with Tom20 and Tom22. Although both $(LARL)_3$ and $(LURL)_3$ form a stable helical conformation, their localization after internalization into the cytosol is markedly different, i.e., they were localized in the vacuoles and the mitochondria, respectively. Since Aib is an amino acid residue substituted with two methyl groups at the α-position, $(LARL)_3$ is supposed to be more hydrophobic than $(LURL)_3$. The hydrophobicity of the peptides was also confirmed in RP-HPLC (Figure S1). Although the purity of the peptides was sufficiently high, two peaks were observed for each peptide due to the isomer of FAM, that is 5- and 6-carboxyfluorescein. The retention time of $(LURL)_3$ was slower than $(LARL)_3$, indicating that $(LURL)_3$ was more hydrophobic than $(LARL)_3$. The helix bundle formation of $(LURL)_3$ indicated

https://dx.doi.org/10.1021/acsbiomaterials.0c01533
ACS Biomater. Sci. Eng. 2021, 7, 1475−1484

by the CD measurement at lower pH (Figure S3) also supports the fact that $(LURL)_3$ tends to cause stronger hydrophobic interactions based on the hydrophobicity of Aib residues. In a similar manner to bundle formation among the single helices, $(LURL)_3$ would bind to Tom20 more strongly via hydrophobic interactions than $(LARL)_3$, resulting in the selective accumulation of $(LURL)_3$ in the mitochondria. The incorporation of Aib residues into the amphiphilic helix consisting of hydrophobic and cationic amino acids improved the efficiency of mitochondrial targeting by increasing both the helical stability and the hydrophobicity.

CONCLUSIONS

We designed artificial mitochondria-targeting peptides with periodic sequences containing a mitochondria-targeting consensus motif and the nonproteinogenic amino acid Aib. We demonstrated that artificial mitochondrial targeting peptides, especially $(LURL)_3$ containing Aib residues, exhibit highly specific accumulating behavior in mitochondria. The CD measurements in combination with simulation studies revealed that the efficient accumulation of $(LURL)_3$ could be ascribed to the formation of an amphiphilic helical conformation that strongly interacts with Tom20. Effective mitochondria targeting would be achieved by virtue of the increased hydrophobicity and stability of the amphiphilic helical conformation, which promote interaction with Tom20 and Tom22, even without MTSs derived from eukaryotic organisms. In addition, the incorporation of Aib into MTSs is expected to improve the long-term stability of the peptides against intracellular enzymes, which is crucial for efficient transformation, especially in plant cells, as well as to increase the hydrophobicity and helical stability of peptides. This is the first report showing effective translocation into plant cell mitochondria using artificial periodic peptides. The novel artificial mitochondria-targeting peptides developed in this study would be beneficial for the selective, efficient modification of plant mitochondria utilizing current peptide-mediated delivery systems into plants.

ASSOCIATED CONTENT

Supporting Information

The Supporting Information is available free of charge at https://pubs.acs.org/doi/10.1021/acsbiomaterials.0c01533.

Contents of secondary structures of the peptides; pH dependence on CD spectra; DLS profiles; secondary structure propensity obtained by GaMD simulations; CLSM images of onion bulb scale leaves for FAM-$(LURR)_3$ and FAM-$(LURS)_3$; and free-energy landscapes for GaMD simulations of the peptides with Tom20 (PDF)

AUTHOR INFORMATION

Corresponding Authors

Kousuke Tsuchiya − *Department of Material Chemistry, Graduate School of Engineering, Kyoto University, Kyoto 615-8510, Japan;* orcid.org/0000-0003-2364-8275; Email: kosuke.3n@kyoto-u.ac.jp

Keiji Numata − *Department of Material Chemistry, Graduate School of Engineering, Kyoto University, Kyoto 615-8510, Japan; Biomacromolecules Research Team, RIKEN Center for Sustainable Resource Science, Wako, Saitama 351-0198, Japan;* orcid.org/0000-0003-2199-7420; Email: keiji.3n@kyoto-u.ac.jp

Authors

Kayo Terada − *Department of Material Chemistry, Graduate School of Engineering, Kyoto University, Kyoto 615-8510, Japan*

Joan Gimenez-Dejoz − *Biomacromolecules Research Team, RIKEN Center for Sustainable Resource Science, Wako, Saitama 351-0198, Japan;* orcid.org/0000-0002-3839-950X

Taichi Kurita − *Department of Material Chemistry, Graduate School of Engineering, Kyoto University, Kyoto 615-8510, Japan*

Kazusato Oikawa − *Department of Material Chemistry, Graduate School of Engineering, Kyoto University, Kyoto 615-8510, Japan*

Hirotaka Uji − *Department of Material Chemistry, Graduate School of Engineering, Kyoto University, Kyoto 615-8510, Japan;* orcid.org/0000-0003-0447-8944

Complete contact information is available at: https://pubs.acs.org/10.1021/acsbiomaterials.0c01533

Author Contributions

K.T. and K.N. conceived and designed the research. K.T., J.G.-D., T.K., K.O., and H.U. performed the experiments and analyzed the data. K.T. and J.G.-D. wrote and K.T. and K.N. edited the manuscript.

Notes

The authors declare no competing financial interest.

ACKNOWLEDGMENTS

The authors acknowledge RIKEN Information System Division for providing access to the Hokusai GreatWave and BigWaterfall supercomputer resources. This work was financially supported by JST ERATO Grant No. JPMJER1602, Japan (K.N.), Grant-in-Aid for Transformative Research Areas (B), and JSPS KAKENHI Grant No. JP20K05718 (K.T.). The authors acknowledge the Support Unit for Bio-Material Analysis, RIKEN Center for Brain Science Research Resources Division, for performing the peptide syntheses.

REFERENCES

(1) Scheffler, I. E. *Mitochondria*; 2nd ed., Wiley-Liss, 2008.
(2) Jacoby, R. P.; Li, L.; Huang, S.; Lee, C. P.; Millar, A. H.; Taylor, N. L. Mitochondrial composition, function and stress response in plants. *J. Integr. Plant Biol.* **2012**, *54*, 887−906.
(3) Oksman-Caldentey, K.-M.; Inzé, D. Plant cell factories in the post-genomic era: new ways to produce designer secondary metabolites. *Trends Plant Sci.* **2004**, *9*, 433−440.
(4) Bohra, A.; Jha, U. C.; Adhimoolam, P.; Bisht, D.; Singh, N. P. Cytoplasmic male sterility (CMS) in hybrid breeding in field crops. *Plant Cell Rep.* **2016**, *35*, 967−993.
(5) Kikkert, J. R.; Vidal, J. R.; Reisch, B. I. Stable Transformation of Plant Cells by Particle Bombardment/Biolistics. In *Transgenic Plants: Methods and Protocols*;Peña, L., Ed.; Methods in Molecular Biology; 2005; Vol. *286*, pp 61−78.
(6) Altpeter, F.; Baisakh, N.; Beachy, R.; Bock, R.; Capell, T.; Christou, P.; Daniell, H.; Datta, K.; Datta, S.; Dix, P. J.; Fauquet, C.; Huang, N.; Kohli, A.; Mooibroek, H.; Nicholson, L.; Nguyen, T. T.; Nugent, G.; Raemakers, K.; Romano, A.; Somers, D. A.; Stoger, E.; Taylor, N.; Visser, R. Particle bombardment and the genetic enhancement of crops: myths and realities. *Mol. Breed.* **2005**, *15*, 305−327.

(7) Klein, T. M.; Arentzen, R.; Lewis, P. A.; Fitzpatrick-McElligott, S. Transformation of Microbes, Plants and Animals by Particle Bombardment. *Nat. Biotechnol.* **1992**, *10*, 286−291.
(8) Merchant, B. Gold, the Noble Metal and the Paradoxes of its Toxicology. *Biologicals* **1998**, *26*, 49−59.
(9) Russell, J. A.; Roy, M. K.; Sanford, J. C. Physical Trauma and Tungsten Toxicity Reduce the Efficiency of Biolistic Transformation. *Plant Physiol.* **1992**, *98*, 1050−1056.
(10) Demirer, G. S.; Zhang, H.; Goh, N. S.; González-Grandío, E.; Landry, M. P. Carbon nanotube-mediated DNA delivery without transgene integration in intact plants. *Nat. Protoc.* **2019**, *14*, 2954−2971.
(11) Ruf, S.; Forner, J.; Hasse, C.; Kroop, X.; Seeger, S.; Schollbach, L.; Schadach, A.; Bock, R. High-efficiency generation of fertile transplastomic *Arabidopsis* plants. *Nat. Plants* **2019**, *5*, 282−289.
(12) Chuah, J.-A.; Yoshizumi, T.; Kodama, Y.; Numata, K. Gene introduction into the mitochondria of *Arabidopsis thaliana* via peptide-based carriers. *Sci. Rep.* **2015**, *5*, No. 7751.
(13) Yoshizumi, T.; Oikawa, K.; Chuah, J.-A.; Kodama, Y.; Numata, K. Selective gene delivery for integrating exogenous DNA into plastid and mitochondrial genomes using peptide−DNA complexes. *Biomacromolecules* **2018**, *19*, 1582−1591.
(14) Chuah, J.-A.; Matsugami, A.; Hayashi, F.; Numata, K. Self-assembled peptide-based system for mitochondrial-targeted gene delivery: functional and structural insights. *Biomacromolecules* **2016**, *17*, 3547−3557.
(15) Schatz, G.; Dobberstein, B. Common principles of protein translocation across membranes. *Science* **1996**, *271*, 1519−1526.
(16) Neupert, W. Protein import into mitochondria. *Annu. Rev. Biochem.* **1997**, *66*, 863−917.
(17) Pfanner, N.; Geissler, A. Versatility of the mitochondrial protein import machinery. *Nat. Rev. Mol. Cell Biol.* **2001**, *2*, 339−349.
(18) Endo, T.; Kohda, D. Functions of outer membrane receptors in mitochondrial protein import. *Biochim. Biophys. Acta, Mol. Cell Res.* **2002**, *1592*, 3−14.
(19) Pfaller, R.; Pfanner, N.; Neupert, W. Mitochondrial protein import. *J. Biol. Chem.* **1989**, *264*, 34−39.
(20) Yamano, K.; Yatsukawa, Y.; Esaki, M.; Hobbs, A. E. A.; Jensen, R. E.; Endo, T. Tom20 and Tom22 share the common signal recognition pathway in mitochondrial protein import. *J. Biol. Chem.* **2008**, *283*, 3799−3807.
(21) Lee, D. W.; Lee, S.; Lee, J.; Woo, S.; Razzak, M. A.; Vitale, A.; Hwang, I. Molecular Mechanism of the Specificity of Protein Import into Chloroplasts and Mitochondria in Plant Cells. *Mol. Plant* **2019**, *12*, 951−966.
(22) Muto, T.; Obita, T.; Abe, Y.; Shodai, T.; Endo, T.; Kohda, D. NMR identification of the Tom20 binding segment in mitochondrial presequences. *J. Mol. Biol.* **2001**, *306*, 137−143.
(23) Demizu, Y.; Doi, M.; Kurihara, M.; Okuda, H.; Nagano, M.; Suemune, H.; Tanaka, M. Conformational studies on peptides containing α,α-disubstituted α-amino acids: chiral cyclic α,α-disubstituted α-amino acid as an α-helical inducer. *Org. Biomol. Chem.* **2011**, *9*, 3303−3312.
(24) Eto, R.; Oba, M.; Ueda, A.; Uku, T.; Doi, M.; Matsuo, Y.; Tanaka, T.; Demizu, Y.; Kurihara, M.; Tanaka, M. Diastereomeric Right- and Left-Handed Helical Structures with Fourteen (R)-Chiral Centers. *Chem. - Eur. J.* **2017**, *23*, 18120−18124.
(25) Crisma, M.; Moretto, A.; Peggion, C.; Panella, L.; Kaptein, B.; Broxterman, Q. B.; Formaggio, F.; Toniolo, C. Chiral, fully extended helical peptides. *Amino Acids* **2011**, *41*, 629−641.
(26) Demizu, Y.; Doi, M.; Kurihara, M.; Maruyama, T.; Suemune, H.; Tanaka, M. One-handed helical screw direction of homopeptide foldamer exclusively induced by cyclic α-amino acid side-chain chiral centers. *Chem. - Eur. J.* **2012**, *18*, 2430−2439.
(27) Crisma, M.; Toniolo, C. Helical screw-sense preferences of peptides based on chiral, Cα-tetrasubstituted α-amino acids. *Biopolymers* **2015**, *104*, 46−64.
(28) Tsuchiya, K.; Numata, K. Chemoenzymatic synthesis of polypeptides containing the unnatural amino acid 2-aminoisobutyric acid. *Chem. Commun.* **2017**, *53*, 7318−7321.
(29) Wada, S.; Hitora, Y.; Tanaka, R.; Urata, H. Translocation of an Aib-containing peptide through cell membranes. *Bioorg. Med. Chem. Lett.* **2008**, *18*, 3999−4001.
(30) Yamashita, H.; Demizu, Y.; Shoda, T.; Sato, Y.; Oba, M.; Tanaka, M.; Kurihara, M. Amphipathic short helix-stabilized peptides with cell-membrane penetrating ability. *Bioorg. Med. Chem.* **2014**, *22*, 2403−2408.
(31) Kato, T.; Oba, M.; Nishida, K.; Tanaka, M. Cell-penetrating helical peptides having l-arginines and five-membered ring α,α-disubstituted α-amino acids. *Bioconjugate Chem.* **2014**, *25*, 1761−1768.
(32) Yamashita, H.; Oba, M.; Misawa, T.; Tanaka, M.; Hattori, T.; Naito, M.; Kurihara, M.; Demizu, Y. A Helix-Stabilized Cell-Penetrating Peptide as an Intracellular Delivery Tool. *ChemBioChem* **2016**, *17*, 137−140.
(33) Yamashita, H.; Kato, T.; Oba, M.; Misawa, T.; Hattori, T.; Ohoka, N.; Tanaka, M.; Naito, M.; Kurihara, M.; Demizu, Y. Development of a Cell-penetrating Peptide that Exhibits Responsive Changes in its Secondary Structure in the Cellular Environment. *Sci. Rep.* **2016**, *6*, No. 33003.
(34) Terada, K.; Gimenez-Dejoz, J.; Miyagi, Y.; Oikawa, K.; Tsuchiya, K.; Numata, K. Artificial Cell-Penetrating Peptide Containing Periodic α-Aminoisobutyric Acid with Long-Term Internalization Efficiency in Human and Plant Cells. *ACS Biomater. Sci. Eng.* **2020**, *6*, 3287−3298.
(35) Obita, T.; Muto, T.; Endo, T.; Kohda, D. Peptide library approach with a disulfide tether to refine the Tom20 recognition motif in mitochondrial presequences. *J. Mol. Biol.* **2003**, *328*, 495−504.
(36) Case, D. A.; Betz, R. M.; Cerutti, D. S.; Cheatham, T. E., III; Darden, T. A.; Duke, R. E.; Giese, T. J.; Gohlke, H.; Goetz, A. W.; Homeyer, N.; Izadi, S.; Janowski, P.; Kaus, J.; Kovalenko, A.; Lee, T. S.; LeGrand, S.; Li, P.; Lin, C.; Luchko, T.; Luo, R.; Madej, B.; Mermelstein, D.; Merz, K. M.; Monard, G.; Nguyen, H.; Nguyen, H. T.; Omelyan, I.; Onufriev, A.; Roe, D. R.; Roitberg, A.; Sagui, C.; Simmerling, C. L.; Botello-Smith, W. M.; Swails, J.; Walker, R. C.; Wang, J.; Wolf, R. M.; Wu, X.; Xiao, L.; Kollman, P. A.*AMBER 2016*, University of California, San Francisco, 2016.
(37) Dupradeau, F.-Y.; Pigache, A.; Zaffran, T.; Savineau, C.; Lelong, R.; Grivel, N.; Lelong, D.; Rosanski, W.; Cieplak, P. The R.E.D. tools: advances in RESP and ESP charge derivation and force field library building. *Phys. Chem. Chem. Phys.* **2010**, *12*, 7821−7839.
(38) Maier, J. A.; Martinez, C.; Kasavajhala, K.; Wickstrom, L.; Hauser, K. E.; Simmerling, C. ff14SB: Improving the Accuracy of Protein Side Chain and Backbone Parameters from ff99SB. *J. Chem. Theory Comput.* **2015**, *11*, 3696−3713.
(39) Jorgensen, W. L.; Chandrasekhar, J.; Madura, J. D.; Impey, R. W.; Klein, M. L. Comparison of simple potential functions for simulating liquid water. *J. Chem. Phys.* **1983**, *79*, 926−935.
(40) Ryckaert, J.-P.; Ciccotti, G.; Berendsen, H. J. C. Numerical integration of the cartesian equations of motion of a system with constraints: molecular dynamics of n-alkanes. *J. Comput. Phys.* **1977**, *23*, 327−341.
(41) Berendsen, H. J. C.; Postma, J. P. M.; van Gunsteren, W. F.; Di Nola, A.; Haak, J. R. Molecular dynamics with coupling to an external bath. *J. Chem. Phys.* **1984**, *81*, 3684−3690.
(42) Essmann, U.; Perera, L.; Berkowitz, M. L.; Darden, T.; Lee, H.; Pedersen, L. G. A smooth particle mesh Ewald method. *J. Chem. Phys.* **1995**, *103*, 8577−8593.
(43) Gotz, A. W.; Williamson, M. J.; Xu, D.; Poole, D.; Le Grand, S.; Walker, R. C. Routine microsecond molecular dynamics simulations with AMBER on GPUs. 1. Generalized born. *J. Chem. Theory Comput.* **2012**, *8*, 1542−1555.
(44) Salomon-Ferrer, R.; Götz, A. W.; Poole, D.; Le Grand, S.; Walker, R. C. Routine microsecond molecular dynamics simulations

https://dx.doi.org/10.1021/acsbiomaterials.0c01533
ACS Biomater. Sci. Eng. 2021, 7, 1475−1484

with AMBER on GPUs. 2. Explicit solvent particle mesh Ewald. *J. Chem. Theory Comput.* **2013**, *9*, 3878−3888.
(45) Le Grand, S.; Götz, A. W.; Walker, R. C. SPFP: Speed without compromise—A mixed precision model for GPU accelerated molecular dynamics simulations. *Comput. Phys. Commun.* **2013**, *184*, 374−380.
(46) Roe, D. R.; Cheatham, T. E., III PTRAJ and CPPTRAJ: software for processing and analysis of molecular dynamics trajectory data. *J. Chem. Theory Comput.* **2013**, *9*, 3084−3095.
(47) Ester, M.; Kriegel, H.-P.; Sander, J.; Xu, X. In *A Density-Based Algorithm for Discovering Clusters in Large Spatial Databases with Noise*, Proceedings of the Second International Conference on Knowledge Discovery and Data Mining (KDD-96), AAAI Press, 1996; pp 226−231.
(48) Komuro, Y.; Miyashita, N.; Mori, T.; Muneyuki, E.; Saitoh, T.; Kohda, D.; Sugita, Y. Energetics of the presequence-binding poses in mitochondrial protein import through Tom20. *J. Phys. Chem. B* **2013**, *117*, 2864−2871.
(49) Srivastava, A.; Tama, F.; Kohda, D.; Miyashita, O. Computational investigation of the conformational dynamics in Tom20-mitochondrial presequence tethered complexes. *Proteins* **2019**, *87*, 81−90.
(50) Miao, Y.; Feher, V. A.; McCammon, J. A. Gaussian accelerated molecular dynamics: Unconstrained enhanced sampling and free energy calculation. *J. Chem. Theory Comput.* **2015**, *11*, 3584−3595.
(51) Miao, Y.; Sinko, W.; Pierce, L.; Bucher, D.; Walker, R. C.; McCammon, J. A. Improved reweighting of accelerated molecular dynamics simulations for free energy calculation. *J. Chem. Theory Comput.* **2014**, *10*, 2677−2689.
(52) Mammi, S.; Rainaldi, M.; Bellanda, M.; Schievano, E.; Peggion, E.; Broxterman, Q. B.; Formaggio, F.; Crisma, M.; Toniolo, C. Concomitant Occurrence of Peptide 310- and α-Helices Probed by NMR. *J. Am. Chem. Soc.* **2000**, *122*, 11735−11736.
(53) Yoder, G.; Polese, A.; Silva, R. A. G. D.; Formaggio, F.; Crisma, M.; Broxterman, Q. B.; Kamphuis, J.; Toniolo, C.; Keiderling, T. A. Conformational Characterization of Terminally Blocked l-(αMe)Val Homopeptides Using Vibrational and Electronic Circular Dichroism. 310-Helical Stabilization by Peptide−Peptide Interaction. *J. Am. Chem. Soc.* **1997**, *119*, 10278−10285.
(54) Toniolo, C.; Polese, A.; Formaggio, F.; Crisma, M.; Kamphuis, J. Circular Dichroism Spectrum of a Peptide 310-Helix. *J. Am. Chem. Soc.* **1996**, *118*, 2744−2745.
(55) Karle, I. L.; Balaram, P. Structural characteristics of alpha-helical peptide molecules containing Aib residues. *Biochemistry* **1990**, *29*, 6747−6756.
(56) Whitmore, L.; Wallace, B. A. DICHROWEB, an online server for protein secondary structure analyses from circular dichroism spectroscopic data. *Nucleic Acids Res.* **2004**, *32*, W668−W673.
(57) Gibson, N. J.; Cassim, J. Y. Evidence for an. alpha. II-type helical conformation for bacteriorhodopsin in the purple membrane. *Biochemistry* **1989**, *28*, 2134−2139.
(58) Ueda, H.; Kimura, S.; Ueda, H.; Imanishi, Y. Incorporation of hydrophobic helix-bundle peptides into lipid bilayer membranes facilitated by a peptide-umbrella structure. *Chem. Commun.* **1998**, *3*, 363−364.
(59) Otoda, K.; Kimura, S.; Imanishi, Y. Orientation and aggregation of hydrophobic helical peptides in phospholipid bilayer membrane. *Biochim. Biophys. Acta, Biomembr.* **1993**, *1150*, 1−8.
(60) Chuah, J.-A.; Numata, K. Stimulus-Responsive Peptide for Effective Delivery and Release of DNA in Plants. *Biomacromolecules* **2018**, *19*, 1154−1163.
(61) Midorikawa, K.; Kodama, Y.; Numata, K. Vacuum/Compression Infiltration-mediated Permeation Pathway of a Peptide-pDNA Complex as a Non-Viral Carrier for Gene Delivery in Planta. *Sci. Rep.* **2019**, *9*, No. 271.
(62) Chugh, A.; Eudes, F.; Shim, Y.-S. Cell-penetrating peptides: Nanocarrier for macromolecule delivery in living cells. *IUBMB Life* **2010**, *62*, 183−193.
(63) Koren, E.; Torchilin, V. P. Cell-penetrating peptides: breaking through to the other side. *Trends Mol. Med.* **2012**, *18*, 385−393.
(64) Martin-Ortigosa, S.; Wang, K. Proteolistics: a biolistic method for intracellular delivery of proteins. *Transgenic Res.* **2014**, *23*, 743−756.

https://dx.doi.org/10.1021/acsbiomaterials.0c01533
ACS Biomater. Sci. Eng. 2021, 7, 1475−1484